Review Article

Diffusion-weighted imaging (DWI) in lymph node staging for prostate cancer

Iztok Caglic[1], Tristan Barrett[2,3]

[1]Department of Radiology, Norfolk & Norwich University Hospital, Norwich, UK; [2]Department of Radiology, [3]CamPARI Clinic, Addenbrooke's Hospital and University of Cambridge, Cambridge, UK

Contributions: (I) Conception and design: All authors; (II) Administrative support: None; (III) Provision of study materials or patients: None; (IV) Collection and assembly of data: All authors; (V) Data analysis and interpretation: None; (VI) Manuscript writing: All authors; (VII) Final approval of manuscript: All authors.

Correspondence to: Iztok Caglic, MD. Department of Radiology, Norfolk & Norwich University Hospital, Colney Lane, Norwich, Norfolk, NR4 7UY, UK. Email: iztok.caglic@nnuh.nhs.uk.

Abstract: In patients with prostate cancer, the presence of lymph node (LN) metastases is a critical prognostic factor and is essential for treatment planning. Conventional cross-sectional imaging performs poorly for nodal staging as both computed tomography (CT) and magnetic resonance imaging (MRI) are mainly dependent on size and basic morphological criteria. Therefore, extended pelvic LN dissection (ePLND) remains the gold standard for LN staging, however, it is an invasive procedure with its own drawbacks, thus creating a need for accurate preoperative imaging test. Incorporating functional MRI by using diffusion-weighted MRI has proven superior to conventional MRI protocol by means of both qualitative and quantitative assessment. Currently, the increased diagnostic performance remains insufficient to replace ePLND and the future role of DWI may be through combination with MR lymphangiography or with novel positron emission tomography (PET) tracers. In this article, the current state of data supporting DWI in LN staging of patients with prostate cancer is discussed.

Keywords: Diffusion-weighted imaging (DWI); lymph nodes (LNs); magnetic resonance imaging (MRI); prostate cancer (PCa); staging

Submitted May 16, 2018. Accepted for publication Aug 02, 2018.
doi: 10.21037/tau.2018.08.04
View this article at: http://dx.doi.org/10.21037/tau.2018.08.04

Introduction

In patients with prostate cancer (PCa), the presence of lymph node (LN) metastases is a key prognostic factor and is essential for treatment planning. Positive LNs are associated with increased biochemical recurrence and metastases, and therefore a higher rate of mortality (1-4). Moreover, the number of involved LNs is one of the strongest predictors of cancer-specific survival, with a favorable prognosis in patients with ≤2 positive LNs (5,6).

Conventional cross-sectional imaging performs poorly for nodal staging as both computed tomography (CT) and magnetic resonance imaging (MRI) are mainly dependent on size and basic morphological criteria, both of which have a poor sensitivity and specificity (7). Therefore, current European Association of Urology (EAU) guidelines recommend extended pelvic LN dissection (ePLND) as the gold standard for LN staging in patients with intermediate and high risk PCa (8). However, ePLND is an invasive procedure, may result in under-sampling, and has a questionable benefit for therapeutic outcome (6,9,10). An accurate noninvasive imaging technique is therefore attractive as a means of overcoming these limitations.

Diffusion-weighted imaging (DWI) is an established imaging modality in the evaluation of primary tumours within the prostate gland (11) and has shown promise for LN staging over and above conventional anatomical MRI sequences. In this article, we focus on the current state

of data supporting DWI in LN staging of patients with PCa and present both the basic principles of DWI and of lymphatic nodal spread.

Pelvic LN groups and lymphatic spread of nodal metastases

PCa disseminates initially and primarily to regional nodes via three pelvic lymphatic drainage pathways, namely the medial chain of the external iliac nodal group, the internal iliac chain, and the pre-sacral route (12). Consequently, four pelvic nodal stations can be involved: the obturator, external and internal iliac, and pre-sacral LNs, which represent regional LNs, with any involved node resulting in "N1" classification. Higher level stations include the common iliac and the para-aortal/paracaval LNs which are considered non-regional nodes and therefore category "M1a" in the TNM classification system (13,14). Prostate MRI is aimed at assessing gland-confined or locally advanced disease, thus the current PI-RADS guidelines only recommend pelvic nodal imaging to the level of the aortic bifurcation (15). A direct ascending pathway of spread is observed with no skip-regions, i.e., the pelvic nodes, followed by the common iliac nodes, and then the retroperitoneal nodes (16). In a recent prospective study Joniau *et al.* performed node mapping in 74 patients with localized PCa, demonstrating that almost all nodal metastases at initial presentation are limited to the pelvis, with the internal iliac group the predominant site (35%) followed by external iliac group (26%) and the obturator fossa group (25%). The remaining positive nodes were distributed between the presacral group (9%), common iliac (3%) or aortic bifurcation group (1%) (10). In addition, a cluster of small regional LNs should be considered highly suspicious for involvement (14).

With a unilateral primary tumour the nodal metastases tend to involve ipsilateral nodal groups, however, contralateral metastases can occur, thus only performing a unilateral/ipsilateral PLND risks under-staging (17). In addition, Tokuda *et al.* showed that in comparison to peripheral zone tumours, anterior index-lesion tumours are much less likely to be associated with LN involvement (18), which might be explained by the dense anterior stroma limiting extra-prostatic spread and a relative paucity of nerves in this location, thereby minimizing the risk of perineural invasion (19,20).

DWI

DWI is a non-invasive imaging technique that reflects the mobility of water molecules in different biologic tissues. There are various DWI techniques available, with echoplanar imaging (EPI) being the most commonly used (21). While free water demonstrates unimpeded movement via Brownian motion, movement is restricted in biologic tissues by their interaction with structures within both the intra- and extra-cellular compartments (22). In addition, these compartments become further reduced in tumours which are composed of multiple cells with enlarged nuclei, increased number of intra-cellular organelles and an increased nucleus-to-cytoplasm ratio resulting in pronounced restricted diffusion of water molecules. DWI is capable of differentiating between fast-moving and slow-moving water protons thus utilizing regional differences in specific diffusion capacities of tissues in order to yield contrast. Signal intensity on DWI is reduced by motion of water protons and vice versa, with reduced movement of water molecules in malignant tissues thus showing high signal on DWI (21-24).

The degree of diffusion sensitization is described by the *b*-value (measured in seconds per square millimetre). Higher *b*-values have a stronger diffusion effect and thus more pronounced signal attenuation, but this comes with an increased noise, reducing the overall signal-to-noise ratio which can limited any incremental benefits (21,25,26). In clinical practice, multiple *b*-values are obtained ranging from 0 to 1,400–2,000 in order to calculate apparent diffusion coefficient (ADC) maps.

The degree of diffusion restriction can be quantitatively expressed by calculating ADC maps, thus allowing tissue characterization. ADC map is typically generated automatically on the scanner as a post-processing step, with acquisition of at least two sequences performed at different *b*-values necessary for its calculation. No optimal *b*-value for DWI assessment of LNs has yet been determined, but most authors suggest imaging with high *b*-values between 800–1,000 s/mm^2 where nodes can be depicted as discrete high signal intensity structures due to their high cellularity (21,25,27). Higher number of *b*-values can further improve the accuracy of calculated ADC but this comes at the expense of increased scanning time (22). To obtain ADC value of a particular lesion one needs to draw regions of interest (ROI) on the map (24). In contrast to raw DWI, where tumours with restricted diffusion appear bright, these are shown as dark on the corresponding ADC map (28). Consequently, tumours tend to exhibit lower ADC values than normal tissues. Nonetheless, different MR units (magnetic field and vendors), different *b*-values used and different methods of calculation (two *vs.* multiple *b*-values) all contribute to

Table 1 Previous ADC mapping studies

Authors	Field strength (T)/ *b*-values (s/mm^2)	No. of patients	Validation method	Metastatic LNs: mean ADC ± SD (in ×10^{-3} mm^2/s)	Non-metastatic LNs: mean ADC ± SD (in ×10^{-3} mm^2/s)
Eiber *et al*. (32)	1.5/50, 300, 600	29[†]	Histopathologic analysis (surgery) or clinical follow-up	1.07±0.23	1.54±0.25*
Beer *et al*. (33)	1.5/50, 300, 600	14[†]	Histopathologic analysis (surgery) or clinical follow-up	1.09±0.23	1.60±0.24*
Vag *et al*. (34)	1.5/50, 300, 600	33[†]	Histopathologic analysis (surgery)	0.96±0.17	1.17±0.22*
Vallini *et al*. (35)	3/500, 800, 1,000, 1,500	26[†]	Histopathologic analysis (surgery)	0.79±0.14	1.13±0.29*
Roy *et al*. (36)	3/0, 1,000	259[‡]	Histopathologic analysis (surgery or biopsy)	0.92±0.22	1.04±0.18
Thoeny *et al*. (37)	3/0, 500, 1,000	120[§]	Histopathologic analysis (surgery)	0.94±0.18	1.01±0.28

*, statistical significance; [†], prostate cancer; [‡], prostate, bladder and penile cancer and gynaecology malignancies; [§], prostate and bladder cancer. LNs, lymph nodes; ADC, apparent diffusion coefficient; SD, standard deviation.

variations in ADC values across institutions (25,27).

Despite several advantages, a major drawback is the potential for susceptibility artefacts to cause both signal loss and image distortion. Susceptibility artefacts result from inhomogeneities of the local magnetic field which in the setting of pelvic imaging occur at the air/soft tissue interface, i.e., adjacent to the gas filled bowel loops (29) and also adjacent to metallic objects such as surgical clips and total hip replacement metalwork. The latter is not so uncommon in the aging population with PCa (30) and can cause non-diagnostic DWI in the gland and obturator region, particularly on the ipsilateral side.

Motion artefacts are another potential concern, although EPI DWI is relatively insensitive when compared to the fast spin echo (FSE) T2-weighted (T2W) imaging (T2WI) and anti-peristaltic drugs such as hyoscine butylbromide or glucagon can be administered in order to decrease bowel peristalsis (31). However, gross motion artefacts which tend to increase with longer scanning times can be problematic, particularly when attempting to measure ADC values of smaller LNs.

ADC mapping studies

Several studies have explored ADC as a potential biomarker in the differentiation of benign from malignant LNs in different organ systems, however, studies in PCa patients are limited and with conflicting results (*Table 1*).

Four studies reported significant differences between ADC values in benign and malignant LNs. Eiber *et al.* assessed 29 patients with PCa and showed that metastatic LNs exhibited lower mean ADC value of (1.07±0.23)×10^{-3} mm^2/s than benign pelvic LNs at (1.54±0.25)×10^{-3} mm^2/s. SA significant difference was observed in both node groups (<10 and ≥10 mm), with receiver operator characteristic-analysis showing superior accuracy of ADC-values (85.6%; sensitivity: 86.0%; specificity: 85.3%) for differentiation of malignant and benign LNs compared to a size-based analysis at a cut-off of 8 mm (accuracy: 66.1%; sensitivity: 82.0%; specificity: 54.4%) (32). A subsequent smaller study by Beer *et al.* including 14 patients with PCa confirmed these findings. Patients were scanned with DW-MR at 1.5 T and ^{11}C-choline-positron emission tomography (PET)/CT, with histopathological correlation available in five patients. Malignant nodes showed significantly lower ADC values than benign nodes at (1.09±0.23)×10^{-3} versus (1.60±0.24)×10^{-3} mm^2/s, respectively. At a cut-off of 1.43×10^{-3} mm^2/s, sensitivity was 96.3%, specificity 78.6%, and accuracy 83.6% on a per-patient basis, with a moderate but highly significant inverse correlation between ADC values and standardized uptake value (SUV) (33). These observations were in agreement with the study by Vag *et al.* who included 33 patients undergoing 1.5T MRI and ^{11}C-choline PET/CT prior to prostatectomy and ePLND. ADC values in malignant LNs were significantly lower at 0.96×10^{-3} mm^2/s *vs.* benign LNs at 1.17×10^{-3} mm^2/s. The optimal cut-off of 1.01×10^{-3} mm^2/s, which was much lower than in a later study, yielded a sensitivity and specificity of 69.7% and 78.6%, respectively (34). Significant differences were also reported in a study including 26 PCa patients with

ADC values of $(0.79\pm0.14)\times10^{-3}$ mm^2/s for metastatic LNs and $(1.13\pm0.29)\times10^{-3}$ mm^2/s for non-involved nodes. Using ADC with an optimal threshold at 0.91×10^{-3} mm^2/s, per-station sensitivity, specificity, positive predictive value (PPV), negative predictive value (NPV) values and diagnostic accuracy were 84.6%, 89.5%, 57.9%, 97.1% and 88.8%, respectively (35).

In contrast, fewer promising results were shown in a study by Roy *et al.* including 259 patients (180 normal, 79 with metastatic prostate, bladder and penile cancer and gynaecology malignancies). They showed no significant difference in the mean ADC value between control common iliac and inguinal nodes and malignant pelvic nodes, although the latter showed mildly lower values at $(0.92\pm0.22)\times10^{-3}$ versus $(1.04\pm0.18)\times10^{-3}$ mm^2/s (36). Similar non-significant findings were reported in a study of 120 patients (87 normal, 33 with metastatic prostate and bladder cancer) with the mean ADC value in metastatic and benign LNs at $(0.94\pm0.18)\times10^{-3}$ and $(1.01\pm0.28)\times10^{-3}$ mm^2/s, respectively (37). A common limitation of the both studies was the lack of homogeneity in the cohort, with multiple tumour types; tumours with differing histological subtypes may differ in cellular architecture which can affect their ADC value, as demonstrated in head and neck malignancies (38). Budiharto *et al.* reported a poor performance of DWI for malignant LN detection in 36 high-risk PCa patients undergoing MRI prior to radical prostatectomy and ePLND, with per-patient sensitivity and specificity of 42.9% and 60%, respectively (39). However, it should be noted that they did not report on ADC values and localised LNs on the *b*-0 s/mm^2, rather than the high-*b*-value images and that no correlation with T2WI was made, potentially allowing both false positive and false negative findings.

Although studies often show a difference in mean ADC value there is a large variation in reported thresholds across studies as well as substantial overlap with non-malignant LNs, due to a multitude of reasons. As shown by Thoeny *et al.*, the amount of metastatic tissue within the node varies significantly (37). Micro metastasis in nodes smaller than 8 mm may show a normal mean ADC value averaged across the node, with this partial voluming effect further accentuated when imaging is performed with a slice thickness at 5 mm or more (25). Another reason may be ROI selection which is particularly important in the setting of necrotic nodes as the areas of necrosis have been shown to significantly increase the ADC value due to their relative fluid composition (40,41). Conversely, certain types of inflammation such as sarcoidosis and cat scratch disease tend to present with a dense fibrous reaction thereby impeding diffusion and lowering ADC values, leading to false positive results (42,43). Similar lowering of ADC values can also be encountered in lipomatosis, follicular hyperplasia and sinus histiocytosis (37). In addition, Kwee *et al.* investigated inter- and intra-observer reproducibility of ADC measurements of LNs in 20 healthy volunteers (in the head and neck and pelvic regions) and concluded that both intra- and inter-observer reproducibility may be insufficient to discriminate malignant from benign LNs (44). Similar studies in primarily mean and median ADC values have been performed in other body organs including prostate with reproducibility ranging from 10–40% (45-49).

Another key reason for literature reported variation is the difference in acquisition protocols. This combined with reproducibility issues and an overlap between benign and malignant ADC values make it difficult to assign an absolute threshold to apply on a per-patient basis. Whilst there is clearly a trend to a lower mean ADC value in metastatic LNs, in contradistinction to PCa within the primary gland where ADC values directly inform decision making, the role of ADC in assessment of nodal status remains debatable.

High-b-value imaging studies/DWI in combination with T2WI

In order to overcome the limitations of quantitative ADC values, some studies have evaluated the diagnostic performance of DWI by means of a qualitative assessment using high-*b*-value images. In all instances this was done in combination with anatomical T2WI (37,50,51).

A study by Mir *et al.* included 20 patients with primary pelvic tumors (4 patients with PCa). Fusion of T2W images with DWI reduced the interpretation time and increased the detection rate of LNs when compared to T2WI alone. T2W identified 114 nodes with a mean diameter of 4.3 mm, whereas 47 additional nodes with a smaller mean diameter of 3.7 mm were detected on fused images, however, the study lacked robust pathological correlation (50). Thoeny *et al.* assessed 120 patients with prostate or bladder cancer undergoing ePLND and staged as N0 by CT or conventional MRI (37). High-*b*-value imaging was used to identify LNs as non-continuous high signal structures which were subsequently carefully assessed for suspicious morphologic criteria on 3D T2WI. On a per-patient level, the reported sensitivities for the two readers were 75.8% and 81.8% with specificity for both being 95.4%. Entry criteria of nodes being negative on conventional imaging selected for nodes of

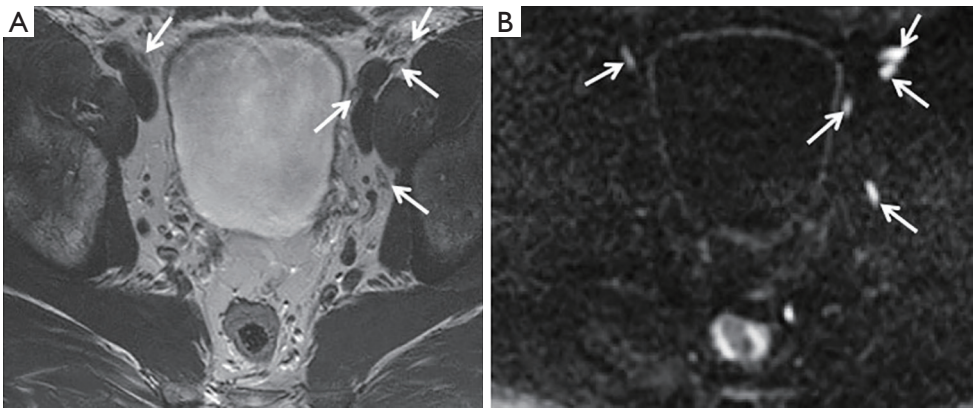

Figure 1 A 68-year-old, PSA 6.3 ng/mL referred for MRI pre-biopsy. No primary tumour detected within the gland. Multiple small volume normal nodes are identified (arrows) on T2-weighted imaging (A), with the nodes being more easily appreciated on the b-1400 diffusion-weighted imaging (B). PSA, prostate-specific antigen; MRI, magnetic resonance imaging.

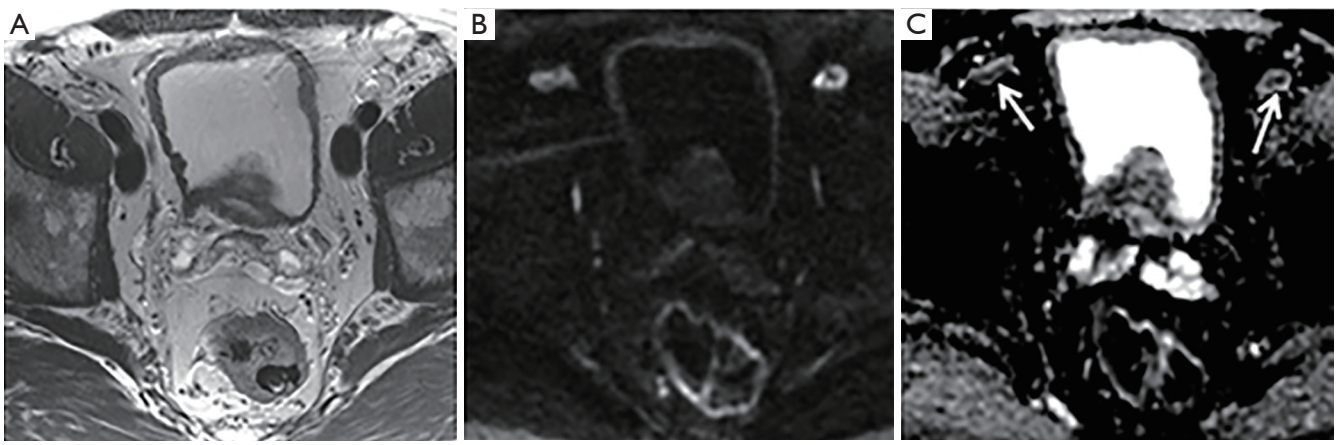

Figure 2 A 74-year-old, PSA 11 ng/mL referred for MRI pre-biopsy. No primary tumour detected, gland volume =125.7 mL. Bilateral external iliac nodes demonstrate benign features with an ovoid shape and fatty hila on T2 (A), b-1400 DWI shows high signal (B), confirmed as "T2-shine through effect" with no restricted diffusion on ADC maps (arrows in C). PSA, prostate-specific antigen; MRI, magnetic resonance imaging; ADC, apparent diffusion coefficient; DWI, diffusion-weighted imaging.

a smaller size, but interestingly, of the 88 positive LNs, the short-axis diameter was less than 5 mm in 60/88 LNs, whilst the maximal metastatic component was 3 mm or less in 46 LNs (37). In another study von Below *et al.* visually assessed LNs in 40 patients with newly diagnosed intermediate- and high-risk PCa who underwent ePLND. Nodes were considered positive when functional criteria (high signal on DWI and low signal on ADC) was accompanied with at least one of standard morphological criteria on T2WI (round, irregular, heterogenous, ill-defined, etc.). Per patient and per regional analysis showed 90% specificity, 55% sensitivity, and 72.5% accuracy and 94% specificity, 41% sensitivity, and 80% accuracy, respectively (51).

Clearly, high-*b*-value imaging is useful in depicting LNs, especially when these do not meet size criteria (*Figure 1*). However, DWI findings need to be carefully correlated with anatomical T2WI in order to avoid false positive results due to structures such as bowel mucosa, vessels and nerves. T2WI should ideally be performed as isovolumetric 3D sequence with thin slice thickness to allow for meticulous analysis of node morphology (37,52). Additionally, it should be noted that nodes regardless of being metastatic or benign exhibit high signal on high-*b*-value imaging, necessitating concurrent evaluation of ADC maps (*Figures 2-5*).

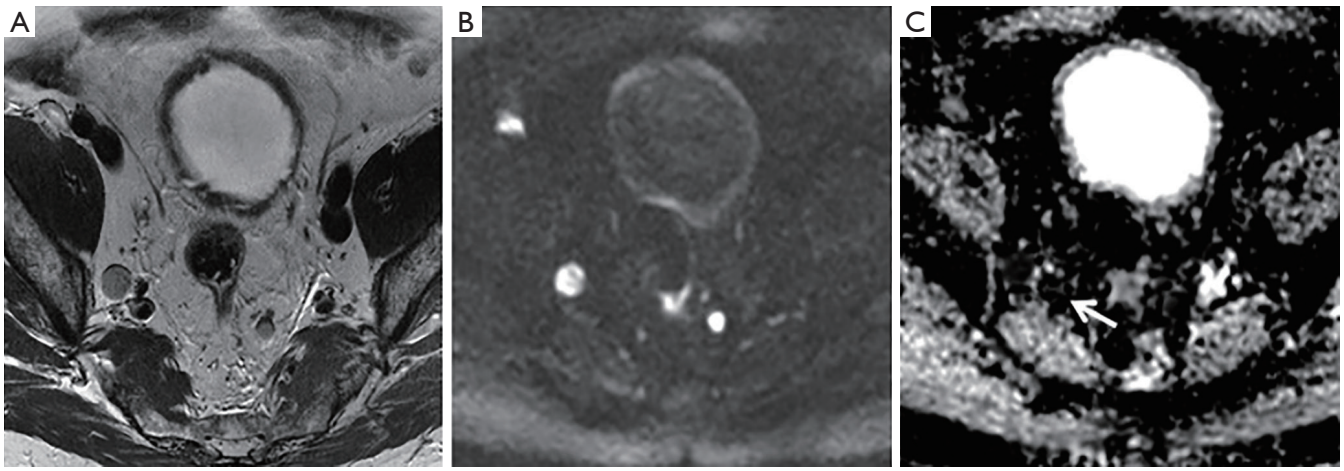

Figure 3 A 71-year-old, PSA 51 ng/mL referred for MRI pre-biopsy. Large volume tumour with extra-capsular extension (not shown), Gleason 4+5 on targeted biopsy. Right and left internal iliac nodes involved, depicted on T2 and b-1400 imaging (A,B), with marked restricted diffusion on ADC maps, value 0.457×10^{-3} $mm^{2/s}$ (arrow) (C). PSA, prostate-specific antigen; MRI, magnetic resonance imaging; ADC, apparent diffusion coefficient.

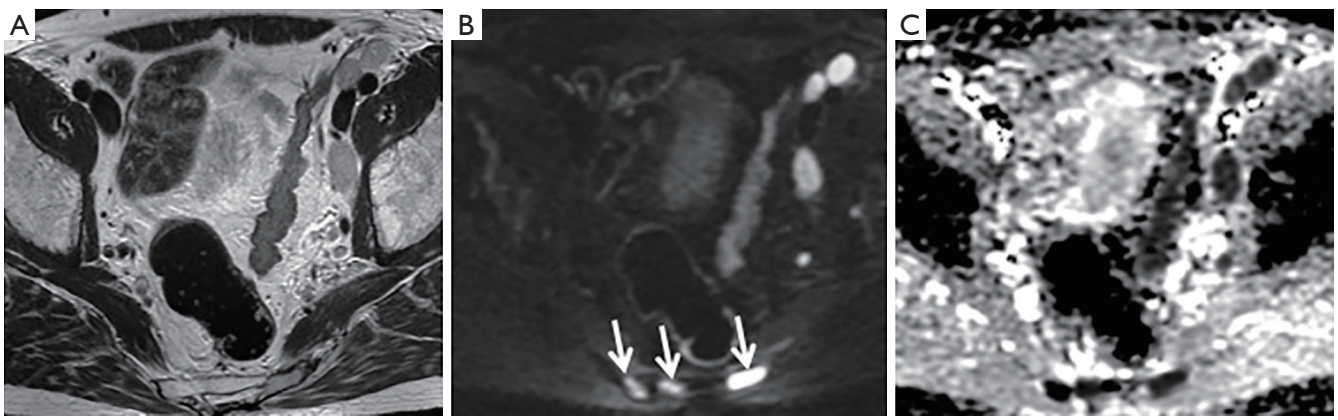

Figure 4 Staging MRI in a 64-year-old patient with biopsy-proven Gleason 4+4 disease. T2-weighted imaging shows a cluster of enlarged left external and internal iliac nodes (A) with restricted diffusion (B,C). Note the high-*b*-value DWI also shows increased conspicuity of bone metastases to the sacrum (arrows). MRI, magnetic resonance imaging; DWI, diffusion-weighted imaging.

DWI in combination with MR lymphography (MRL)

MRL with ultrasmall superparamagnetic iron oxide (USPIO) has shown promising results in depicting nodal disease in PCa (53,54). Several other body regions have also been studied, with a meta-analysis showing the pooled sensitivity and specificity of the technique for nodal metastatic involvement to be 90% and 96%, respectively (55). Unfortunately, USPIO is currently not widely available following withdrawal of its licence in many regions, currently only being produced in the Netherlands (commercially known as Combidex) where its use is mainly limited to research purposes in patients with PCa (56).

USPIO nanoparticles need to be administered intravenously 24–36 h prior to MRI imaging. During this time, they are taken up by numerous macrophages which are present within normal LNs, but do not accumulate within metastatic nodes as they lack macrophages. Deposition of iron oxide within the normal nodes results in signal decrease on T2W and T2*W MRI whereas metastatic nodes will retain its baseline signal intensity (53,54). However, one of the major limitations to the

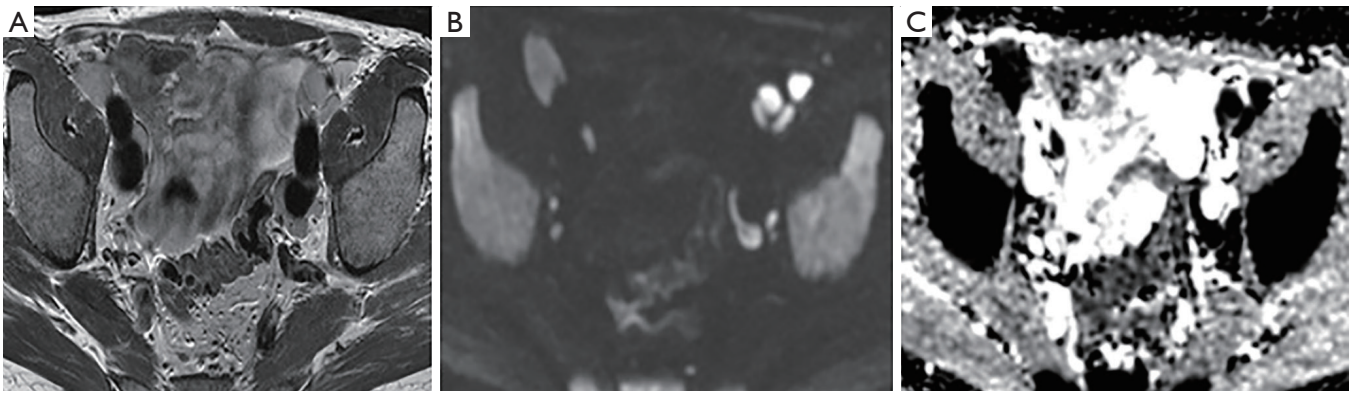

Figure 5 A 64-year-old patient on active surveillance with stable PSA. Transperineal biopsy 2 years prior showed 1/24 cores positive for Gleason 3+3 disease (<5%). No convincing lesion demonstrated in the prostate on MRI. T2-weighted imaging shows new adenopathy (A) with associated restricted diffusion (B,C) and heterogeneous bone marrow change. Nodal distribution involving inguinal nodes and iliac chains but not obturator regions. Nodal biopsy showed B-cell lymphoma with immunophenotype in keeping with CLL/SLL. MRI, magnetic resonance imaging; PSA, prostate-specific antigen; CLL, chronic lymphocytic leukemia; SLL, small lymphocytic lymphoma.

widespread use of USPIO is the need for pre- and post-contrast imaging for comparison purposes, necessitating two MR examinations on consecutive days and increasing costs.

Adding DWI to the MRL may be of further benefit as high-*b*-value imaging is affected in the same manner as T2WI due to USPIO's effect of significantly reducing T2 relaxation. Although this is in principle a negative contrast agent, uptake in normal LNs results in signal loss, meaning the abnormal nodes retain a hyperintense signal, thus being well depicted on DWI. Thoeny *et al.* and Birkhäuser *et al.* used this approach with a DWI sequence covering the entire pelvis, reporting sensitivities between 65–75% and specificities of 93–96% (57,58). These results were however inferior to the above-mentioned meta-analysis (55), with one potential explanation being their use of a T2W instead of a T2*W sequence (59). Nonetheless, additional benefits of their protocol were the need for only one MRI session and faster acquisition, as well as easier image interpretation and shorter reading time (57).

Incorporating DWI in MRI protocols has proven superior to conventional cross-sectional imaging. Quantitative assessment has shown inconsistent results and whilst the ADC values of metastatic LNs are lower than those of benign nodes, there is a significant overlap and variations in the literature-reported thresholds. Improved diagnostic performance can be achieved by means of qualitative evaluation of high-*b*-value imaging, which should ideally serve as a nodal map to depict nodes, which then warrant careful correlation and assessment on anatomical T2WI. Currently, the increased sensitivity of these approaches is not sufficient to fully replace ePLND and negative MRI findings should therefore not deter urologists from nodal dissection if this is otherwise clinically indicated. The future role of DWI may be in combination with USPIO-enhanced MR imaging or novel PET agents, such as prostate-specific membrane antigen (PSMA), however, a sufficient number of high quality studies are required before imaging can fully replace ePLND in clinical practice.

Summary

Accurate nodal staging is vital for prognosis and treatment planning in patients with PCa. Both CT and conventional MRI have poor sensitivity and specificity for assessment due to their over-reliance on size criteria. Although ePLND remains the gold standard for LN staging, it has disadvantages, creating a need for accurate preoperative imaging test.

Acknowledgements

Author T Barrett acknowledges support from Cancer Research UK, National Institute of Health Research Cambridge Biomedical Research Centre, Cancer Research UK and the Engineering and Physical Sciences Research Council Imaging Centre in Cambridge and Manchester and the Cambridge Experimental Cancer Medicine Centre.

Footnote

Conflicts of Interest: The authors have no conflicts of interest to declare.

References

1. Bader P, Burkhard FC, Markwalder R, et al. Disease progression and survival of patients with positive lymph nodes after radical prostatectomy. Is there a chance of cure? J Urol 2003;169:849-54.
2. Verhagen PC, Schröder FH, Collette L, et al. Does local treatment of the prostate in advanced and/or lymph node metastatic disease improve efficacy of androgen-deprivation therapy? A systematic review. Eur Urol 2010;58:261-9.
3. Eggener SE, Scardino PT, Walsh PC, et al. Predicting 15-year prostate cancer specific mortality after radical prostatectomy. J Urol 2011;185:869-75.
4. Touijer KA, Karnes RJ, Passoni N, et al. Survival Outcomes of Men with Lymph Node-positive Prostate Cancer After Radical Prostatectomy: A Comparative Analysis of Different Postoperative Management Strategies. Eur Urol 2018;73:890-6.
5. Ledezma RA, Negron E, Razmaria AA, et al. Robotic-assisted pelvic lymph node dis- section for prostate cancer: frequency of nodal metastases and oncological outcomes. World J Urol 2015;33:1689-94.
6. Briganti A, Blute ML, Eastham JH, et al. Pelvic lymph node dissection in prostate cancer. Eur Urol 2009;55:1251-65.
7. Hövels AM, Heesakkers RA, Adang EM, et al. The diagnostic accuracy of CT and MRI in the staging of pelvic lymph nodes in patients with prostate cancer: a meta-analysis. Clin Radiol 2008;63:387-95.
8. Mottet N, Bellmunt J, Briers E, et al. Guidelines on Prostate Cancer. Accessed May 2018. Available online: https://uroweb.org/guideline/prostate-cancer/
9. Fossati N, Willemse PM, Van den Broeck T, et al. The Benefits and Harms of Different Extents of Lymph Node Dissection During Radical Prostatectomy for Prostate Cancer: A Systematic Review. Eur Urol 2017;72:84-109.
10. Joniau S, Van den Bergh L, Lerut E, et al. Mapping of pelvic lymph node metastases in prostate cancer. Eur Urol 2013;63:450-8.
11. Barrett T, Turkbey B, Choyke PL. PI-RADS version 2: what you need to know. Clin Radiol 2015;70:1165-76.
12. Paño B, Sebastià C, Buñesch L, et al. Pathways of lymphatic spread in male urogenital pelvic malignancies. Radiographics 2011;31:135-60.
13. Brierley JD, Gospodarowicz MK, Wittekind C. TNM classification of malignant tumors. 8th edition. Wiley-Blackwell, 2016.
14. McMahon CJ, Rofsky NM, Pedrosa I. Lymphatic metastases from pelvic tumors: anatomic classification, characterization, and staging. Radiology 2010;254:31-46.
15. Weinreb JC, Barentsz JO, Choyke PL, et al. PI-RADS Prostate Imaging - Reporting and Data System: 2015, Version 2. Eur Urol 2016;69:16-40.
16. Briganti A, Suardi N, Capogrosso P, et al. Lymphatic spread of nodal metastases in high-risk prostate cancer: The ascending pathway from the pelvis to the retroperitoneum. Prostate 2012;72:186-92.
17. Weckermann D, Holl G, Dorn R, et al. Reliability of preoperative diagnostics and location of lymph node metastases in presumed unilateral prostate cancer. BJU Int 2007;99:1036-40.
18. Tokuda Y, Carlino LJ, Gopalan A, et al. Prostate cancer topography and patterns of lymph node metastasis. Am J Surg Pathol 2010;34:1862-7.
19. McNeal JE. Cancer volume and site of origin of adenocarcinoma in the prostate: relationship to local and distant spread. Hum Pathol 1992;23:258-66.
20. Villers A, McNeal JE, Redwine EA, et al. The role of perineural space invasion in the local spread of prostatic adenocarcinoma. J Urol 1989;142:763-8.
21. Qayyum A. Diffusion-weighted imaging in the abdomen and pelvis: concepts and applications. Radiographics 2009;29:1797-810.
22. Koh DM, Collins DJ. Diffusion-weighted MRI in the body: applications and challenges in oncology. AJR Am J Roentgenol 2007;188:1622-35.
23. Iima M, Le Bihan D. Clinical Intravoxel Incoherent Motion and Diffusion MR Imaging: Past, Present, and Future. Radiology 2016;278:13-32.
24. Malayeri AA, El Khouli RH, Zaheer A, et al. Principles and applications of diffusion-weighted imaging in cancer detection, staging, and treatment follow-up. Radiographics 2011;31:1773-91.
25. Herneth AM, Mayerhoefer M, Schernthaner R, et al. Diffusion weighted imaging: lymph nodes. Eur J Radiol 2010;76:398-406.
26. Saremi F, Knoll AN, Bendavid OJ, et al. Characterization of genitourinary lesions with diffusion-weighted imaging. Radiographics 2009;29:1295-317.
27. Thoeny HC, Barbieri S, Froehlich JM, et al. Functional and Targeted Lymph Node Imaging in Prostate Cancer:

Current Status and Future Challenges. Radiology 2017;285:728-43.
28. Le Bihan D, Breton E, Lallemand D, et al. Separation of diffusion and perfusion in intravoxel incoherent motion MR imaging. Radiology 1988;168:497-505.
29. Caglic I, Hansen NL, Slough RA, et al. Evaluating the effect of rectal distension on prostate multiparametric MRI image quality. Eur J Radiol 2017;90:174-80.
30. Czarniecki M, Caglic I, Grist JT, et al. Role of PROPELLER-DWI of the prostate in reducing distortion and artefact from total hip replacement metalwork. Eur J Radiol 2018;102:213-9.
31. Gutzeit A, Binkert CA, Koh DM, et al. Evaluation of the anti-peristaltic effect of glucagon and hyoscine on the small bowel: comparison of intravenous and intramuscular drug administration. Eur Radiol 2012;22:1186-94.
32. Eiber M, Beer AJ, Holzapfel K, et al. Preliminary results for characterization of pelvic lymph nodes in patients with prostate cancer by diffusion-weighted MR-imaging. Invest Radiol 2010;45:15-23.
33. Beer AJ, Eiber M, Souvatzoglou M, et al. Restricted water diffusibility as measured by diffusion-weighted MR imaging and choline uptake in (11)C-choline PET/CT are correlated in pelvic lymph nodes in patients with prostate cancer. Mol Imaging Biol 2011;13:352-61.
34. Vag T, Heck MM, Beer AJ, et al. Preoperative lymph node staging in patients with primary prostate cancer: comparison and correlation of quantitative imaging parameters in diffusion-weighted imaging and 11C-choline PET/CT. Eur Radiol 2014;24:1821-6.
35. Vallini V, Ortori S, Boraschi P, et al. Staging of pelvic lymph nodes in patients with prostate cancer: Usefulness of multiple b value SE-EPI diffusion-weighted imaging on a 3.0 T MR system. Eur J Radiol Open 2015;3:16-21.
36. Roy C, Bierry G, Matau A, et al. Value of diffusion-weighted imaging to detect small malignant pelvic lymph nodes at 3 T. Eur Radiol 2010;20:1803-11.
37. Thoeny HC, Froehlich JM, Triantafyllou M, et al. Metastases in normal-sized pelvic lymph nodes: detection with diffusion-weighted MR imaging. Radiology 2014;273:125-35.
38. Pekçevik Y, Çukurova İ, Arslan İB. Apparent diffusion coefficient for discriminating metastatic lymph nodes in patients with squamous cell carcinoma of the head and neck. Diagn Interv Radiol 2015;21:397-402.
39. Budiharto T, Joniau S, Lerut E, et al. Prospective evaluation of 11C-choline positron emission tomography/computed tomography and diffusion-weighted magnetic resonance imaging for the nodal staging of prostate cancer with a high risk of lymph node metastases. Eur Urol 2011;60:125-30.
40. Herneth AM, Guccione S, Bednarski M. Apparent diffusion coefficient: a quantitative parameter for in vivo tumor characterization. Eur J Radiol 2003;45:208-13.
41. Sumi M, Van Cauteren M, Nakamura T. MR microimaging of benign and malignant nodes in the neck. AJR Am J Roentgenol 2006;186:749-57.
42. Abdel Razek AA, Soliman NY, Elkhamary S, et al. Role of diffusion-weighted MR imaging in cervical lymphadenopathy. Eur Radiol 2006;16:1468-77.
43. Muenzel D, Duetsch S, Fauser C, et al. Diffusion-weighted magnetic resonance imaging in cervical lymphadenopathy: report of three cases of patients with Bartonella henselae infection mimicking malignant disease. Acta Radiol 2009;50:914-6.
44. Kwee TC, Takahara T, Luijten PR, et al. ADC measurements of lymph nodes: inter- and intra-observer reproducibility study and an overview of the literature. Eur J Radiol 2010;75:215-20.
45. Braithwaite AC, Dale BM, Boll DT, et al. Short- and midterm reproducibility of apparent diffusion coefficient measurements at 3.0-T diffusion-weighted imaging of the abdomen. Radiology 2009;250:459-65.
46. Rosenkrantz AB, Oei M, Babb JS, et al. Diffusion-weighted imaging of the abdomen at 3.0 Tesla: image quality and apparent diffusion coefficient reproducibility compared with 1.5 Tesla. J Magn Reson Imaging 2011;33:128-35.
47. Miquel ME, Scott AD, Macdougall ND, et al. In vitro and in vivo repeatability of abdominal diffusion-weighted MRI. Br J Radiol 2012;85:1507-12.
48. Sadinski M, Medved M, Karademir I, et al. Short-term reproducibility of apparent diffusion coefficient estimated from diffusion-weighted MRI of the prostate. Abdom imaging 2015;40:2523-8.
49. Fedorov A, Vangel MG, Tempany CM, et al. Multiparametric Magnetic Resonance Imaging of the Prostate: Repeatability of Volume and Apparent Diffusion Coefficient Quantification. Invest Radiol 2017;52:538-46.
50. Mir N, Sohaib SA, Collins D, et al. Fusion of high b-value diffusion-weighted and T2-weighted MR images improves identification of lymph nodes in the pelvis. J Med Imaging Radiat Oncol 2010;54:358-64.
51. von Below C, Daouacher G, Wassberg C, et al. Validation of 3 T MRI including diffusion-weighted imaging for nodal staging of newly diagnosed intermediate- and high-risk prostate cancer. Clin Radiol 2016;71:328-34.

52. Barentsz JO, Richenberg J, Clements R, et al. ESUR prostate MR guidelines 2012. Eur Radiol 2012;22:746-57.
53. Harisinghani MG, Saini S, Weissleder R, et al. MR lymphangiography using ultrasmall superparamagnetic iron oxide in patients with primary abdominal and pelvic malignancies: radiographic-pathologic correlation. AJR Am J Roentgenol 1999;172:1347-51.
54. Harisinghani MG, Barentsz J, Hahn PF, et al. Noninvasive detection of clinically occult lymph-node metastases in prostate cancer. N Engl J Med 2003;348:2491-9. Erratum in: N Engl J Med 2003;349:1010.
55. Wu L, Cao Y, Liao C, et al. Diagnostic performance of USPIO-enhanced MRI for lymph-node metastases in different body regions: a meta-analysis. Eur J Radiol 2011;80:582-9.
56. Fortuin AS, Brüggemann R, van der Linden J, et al. Ultrasmall superparamagnetic iron oxides for metastatic lymph node detection: back on the block. Wiley Interdiscip Rev Nanomed Nanobiotechnol 2018;10. doi: 10.1002/wnan.1471.
57. Birkhäuser FD, Studer UE, Froehlich JM, et al. Combined ultrasmall superparamagnetic particles of iron oxide-enhanced and diffusion-weighted magnetic resonance imaging facilitates detection of metastases in normal-sized pelvic lymph nodes of patients with bladder and prostate cancer. Eur Urol 2013;64:953-60.
58. Thoeny HC, Triantafyllou M, Birkhaeuser FD, et al. Combined ultrasmall superparamagnetic particles of iron oxide-enhanced and diffusion- weighted magnetic resonance imaging reliably detect pelvic lymph node metastases in normal-sized nodes of bladder and prostate cancer patients. Eur Urol 2009;55:761-9.
59. Fortuin AS, Barentsz JO. Comments on Ultrasmall superparamagnetic particles of iron oxide allow for the detection of metastases in normal sized pelvic lymph nodes of patients with bladder and/or prostate cancer, Triantafyllou et al., European Journal of Cancer, published online 22 October 2012. Eur J Cancer 2013;49:1789-90.

Cite this article as: Caglic I, Barrett T. Diffusion-weighted imaging (DWI) in lymph node staging for prostate cancer. Transl Androl Urol 2018;7(5):814-823. doi: 10.21037/tau.2018.08.04

